Numerical simulation of wave propagation in frozen porous media*

José M. Carcione† Géza Seriani‡

Abstract

We propose a numerical algorithm for simulating wave propagation in frozen porous media. The original theory assumes that there is no direct contact between solid grains and ice (we include the grain-ice interaction), and predicts three compressional waves and two shear waves. The wavefield is obtained with a grid-method based on the Fourier differential operator and a 4th-order Runge-Kutta time-integration algorithm. Since the presence of slow diffusive waves makes the differential equations stiff, a time-splitting integration algorithm is used to solved the stiff part with an analytical technique.

1 Introduction

Knowledge of the physical properties of frozen soils is essential for the exploitation of mineral resources in polar areas and quantification of the amount of drilling necessary for the construction of highways and pipelines. Another recent application concerns bottom simulating reflectors (BSR), which are shallow seismic anomalies caused by gas-hydrate sediments trapping underlying free gas bearing sediments partially saturated with water. These applications require the knowledge of the degree of freezing of the interstitial water and the amount of free gas. They have a negligible effect on density and magnetic permeability, precluding the use of gravimetric and magnetic techniques, but have a remarkable effect on wave velocities [2]. Hence, seismic and acoustic logging methods constitute the best way for quantifying the amount of ice and water.

A three-phase theory based on first principles has been recently proposed by Leclaire et al. [6]. The theory, which assumes that there is no direct contact between solid grains and ice, predicts three compressional waves and two shear waves and can be applied to unconsolidated and consolidated media. Leclaire et al. [6] also provide a thermodynamic relation between water proportion and temperature. We modify the theory to include grain-ice interaction and grain cementation with decreasing temperature. Snapshots are obtained by solving the equations of motion with a direct-grid algorithm based on the Fourier pseudospectral method for computing the spatial derivatives. Time-splitting [1] allows us to model the diffusive modes.

*This work was partly supported by the European Union under the project *Detection of overpressure zones with seismic and well data.*

†Istituto Nazionale di Oceanografia e di Geofisica Sperimentale, Trieste, Italy, e-mail: jcarcione@ogs.trieste.it

‡e-mail: gseriani@ogs.trieste.it

2 Frozen porous medium

Leclaire et al. [6] assume that there is no direct contact between solid and ice. We have included this contribution to the potential and kinetic energies, and the stiffening of the skeleton due to grain cementation at freezing temperatures.

The equations of momentum conservation are deduced using Lagrange's equations:

$$
\begin{aligned}
&\sigma^{(1)}_{ix,x} + \sigma^{(1)}_{iz,z} = \rho_{11}\dot{v}_i^{(1)} + \rho_{12}\dot{v}_i^{(2)} \underline{+ \rho_{13}\dot{v}_i^{(3)}} - b_{12}(v_i^{(2)} - v_i^{(1)}) \underline{- b_{13}(v_i^{(3)} - v_i^{(1)})},\\
&\sigma^{(2)}_{,i} = \rho_{12}\dot{v}_i^{(1)} + \rho_{22}\dot{v}_i^{(2)} + \rho_{23}\dot{v}_i^{(3)} + b_{12}(v_i^{(2)} - v_i^{(1)}) + b_{23}(v_i^{(2)} - v_i^{(3)}),\\
&\sigma^{(3)}_{ix,x} + \sigma^{(3)}_{iz,z} = \underline{\rho_{13}\dot{v}_i^{(1)}} + \rho_{23}\dot{v}_i^{(2)} + \rho_{33}\dot{v}_i^{(3)} - b_{23}(v_i^{(2)} - v_i^{(3)}) \underline{+ b_{13}(v_i^{(3)} - v_i^{(1)})},
\end{aligned}
\tag{1}
$$

where σ are stress components, v are particle velocities, ρ are density components, and b are friction coefficients [2, 6]; superscripts 1,2 and 3 refer to solid grain, water and ice, respectively, and index i indicates the Cartesian components x and z. A dot above a variable denotes time differentiation.

The 2-D constitutive equations, with the addition of the terms corresponding to grain-ice interaction in the potential energy are

$$
\begin{aligned}
&\sigma^{(1)}_{xx} = (K_1 + \mu_1)\epsilon^{(1)}_{xx} + (K_1 - \mu_1)\epsilon^{(1)}_{zz} + C_{12}\theta_2 + (C_{13} \underline{+ \tfrac{1}{2}\mu_{13}})\epsilon^{(3)}_{xx} + (C_{13} \underline{- \tfrac{1}{2}\mu_{13}})\epsilon^{(3)}_{zz},\\
&\sigma^{(1)}_{zz} = (K_1 + \mu_1)\epsilon^{(1)}_{zz} + (K_1 - \mu_1)\epsilon^{(1)}_{xx} + C_{12}\theta_2 + (C_{13} \underline{+ \tfrac{1}{2}\mu_{13}})\epsilon^{(3)}_{zz} + (C_{13} \underline{- \tfrac{1}{2}\mu_{13}})\epsilon^{(3)}_{xx},\\
&\sigma^{(1)}_{xz} = 2\mu_1\epsilon^{(1)}_{xz} \underline{+ \mu_{13}\epsilon^{(3)}_{xz}},\\
&\\
&\sigma^{(2)} = C_{12}(\epsilon^{(1)}_{xx} + \epsilon^{(1)}_{zz}) + K_2\theta_2 + C_{23}(\epsilon^{(3)}_{xx} + \epsilon^{(3)}_{zz}),\\
&\sigma^{(3)}_{xx} = (K_3 + \mu_3)\epsilon^{(3)}_{xx} + (K_3 - \mu_3)\epsilon^{(3)}_{zz} + C_{23}\theta_2 + (C_{13} \underline{+ \tfrac{1}{2}\mu_{13}})\epsilon^{(1)}_{xx} + (C_{13} \underline{- \tfrac{1}{2}\mu_{13}})\epsilon^{(1)}_{zz},\\
&\sigma^{(3)}_{zz} = (K_3 + \mu_3)\epsilon^{(3)}_{zz} + (K_3 - \mu_3)\epsilon^{(3)}_{xx} + C_{23}\theta_2 + (C_{13} \underline{+ \tfrac{1}{2}\mu_{13}})\epsilon^{(1)}_{zz} + (C_{13} \underline{- \tfrac{1}{2}\mu_{13}})\epsilon^{(1)}_{xx},\\
&\sigma^{(3)}_{xz} = 2\mu_3\epsilon^{(3)}_{xz} \underline{+ \mu_{13}\epsilon^{(1)}_{xz}},\\
&\\
&\theta_2 = \epsilon^{(2)}_{xx} + \epsilon^{(2)}_{zz},
\end{aligned}
\tag{2}
$$

where ϵ are strain components and K, μ and C are stiffnesses [2, 6]. The underlined terms in equations (1) and (2) correspond to the extension of the theory.

The numerical solution of equations (1) and (2) is obtained by a velocity-stress formulation. This results in first-order (in space and time) differential equations, where the unknown variables are the particle velocities and stress components. The equations of momentum conservation can be rewritten as

$$
\begin{aligned}
\dot{v}_i^{(1)} &= \gamma_{11}\Pi_i^{(1)} + \gamma_{12}\Pi_i^{(2)} + \gamma_{13}\Pi_i^{(3)},\\
\dot{v}_i^{(2)} &= \gamma_{12}\Pi_i^{(1)} + \gamma_{22}\Pi_i^{(2)} + \gamma_{23}\Pi_i^{(3)},\\
\dot{v}_i^{(3)} &= \gamma_{13}\Pi_i^{(1)} + \gamma_{23}\Pi_i^{(2)} + \gamma_{33}\Pi_i^{(3)},
\end{aligned}
\tag{3}
$$

where

$$
\begin{aligned}
\Pi_i^{(1)} &= \sigma^{(1)}_{ix,x} + \sigma^{(1)}_{iz,z} + b_{12}(v_i^{(2)} - v_i^{(1)}) + b_{13}(v_i^{(3)} - v_i^{(1)}),\\
\Pi_i^{(2)} &= \sigma^{(2)}_{,i} - b_{12}(v_i^{(2)} - v_i^{(1)}) - b_{23}(v_i^{(2)} - v_i^{(3)}),\\
\Pi_i^{(3)} &= \sigma^{(3)}_{ix,x} + \sigma^{(3)}_{iz,z} + b_{23}(v_i^{(2)} - v_i^{(3)}) - b_{13}(v_i^{(3)} - v_i^{(1)})
\end{aligned}
\tag{4}
$$

are the rate of generalized momenta, and γ_{nm} are the components of the following symmetric matrix

$$\begin{pmatrix} \rho_{11} & \rho_{12} & \rho_{13} \\ \rho_{12} & \rho_{22} & \rho_{23} \\ \rho_{13} & \rho_{23} & \rho_{33} \end{pmatrix}^{-1}. \tag{5}$$

The equations corresponding to the stress components are obtained by time differentiating equations (2) and noting that the rate of the strain components is

$$\dot{\epsilon}_{ij}^{(m)} = \frac{1}{2}(v_{i,j}^{(m)} + v_{j,i}^{(m)}).$$

3 Numerical algorithm

The velocity-stress differential equations can be written in matrix form as

$$\dot{\mathbf{w}} = \mathbf{M}\mathbf{w} + \mathbf{s}, \tag{6}$$

where

$$\mathbf{w} = [v_x^{(1)}, v_x^{(2)}, v_x^{(3)}, v_z^{(1)}, v_z^{(2)}, v_z^{(3)}, \sigma_{xx}^{(1)}, \sigma_{zz}^{(1)}, \sigma_{xz}^{(1)}, \sigma^{(2)}, \sigma_{xx}^{(3)}, \sigma_{zz}^{(3)}, \sigma_{xz}^{(3)}]^\top, \tag{7}$$

is the unknown velocity-stress vector,

$$\mathbf{s} = [0, 0, 0, 0, 0, 0, s_{xx}^{(1)}, s_{zz}^{(1)}, s_{xz}^{(1)}, s^{(2)}, s_{xx}^{(3)}, s_{zz}^{(3)}, s_{xz}^{(3)}]^\top \tag{8}$$

is the source vector, and $\mathbf{M}$ is the propagation matrix containing the spatial derivatives and material properties.

For application of the source, we consider three main cases: i) Frame sources: $s^{(2)} = 0$, and the various combinations of $s_{xx}^{(m)}$, $s_{zz}^{(m)}$ and $s_{xz}^{(m)}$ giving a horizontal force, a vertical force, an explosive source and a pure shear source, all applied to the rock-frame (m=1) or to the ice-matrix (m=3); ii) Fluid volume injection: the matrix sources are equal to zero, and $s^{(2)} \neq 0$; iii) Bulk source: this case assumes that the energy is partitioned between the three phases and that the shear sources vanish; that is, $s_{xx}^{(1)} = s_{zz}^{(1)} = s^{(2)} = s_{xx}^{(3)} = s_{zz}^{(3)}$.

The eigenvalues of $\mathbf{M}$ have negative real parts and differ greatly in magnitude due to the terms containing the friction coefficients b_{12} and b_{23}. The presence of large eigenvalues, together with small eigenvalues, indicates that the problem is *stiff* [4]. The differential equations are solved with the splitting algorithm introduced by Carcione and Quiroga-Goode [1] for propagation in two-phase poroacoustic media, generalized here for three-phase porous media. The propagation matrix can be partitioned as

$$\mathbf{M} = \mathbf{M}_r + \mathbf{M}_s, \tag{9}$$

where $\mathbf{M}_r$ and $\mathbf{M}_s$ correspond to the regular and stiff parts of the differential equations, respectively. The wavefield is advanced with a time step dt and computed using a second-order accurate product formula of the evolution operator

$$\exp(\mathbf{M}dt) = \exp\left(\frac{1}{2}\mathbf{M}_s dt\right) \exp(\mathbf{M}_r dt) \exp\left(\frac{1}{2}\mathbf{M}_s dt\right). \tag{10}$$

Equation (10) allow us to solve the stiff part separately. Using the *Kronecker product* "$\otimes$" of two matrices yields

$$\mathbf{M}_s = \begin{pmatrix} \mathbf{I}_2 \otimes \mathbf{S} & \mathbf{0} \\ \mathbf{0} & \mathbf{0} \end{pmatrix}. \tag{11}$$

with $\mathbf{I}_2$ the (2×2) identity matrix. We should solve

$$\dot{\mathbf{v}}_i = \mathbf{S}\mathbf{v}_i, \tag{12}$$

for each Cartesian component i, where

$$\mathbf{v}_i = [v_i^{(1)}, v_i^{(2)}, v_i^{(3)}]^\top, \tag{13}$$

and

$$\begin{aligned}
\mathbf{S}_{11} &= b_{12}(\gamma_{12} - \gamma_{11}) + b_{13}(\gamma_{13} - \gamma_{11}),\\
\mathbf{S}_{12} &= b_{12}(\gamma_{11} - \gamma_{12}) + b_{23}(\gamma_{13} - \gamma_{12}),\\
\mathbf{S}_{13} &= b_{23}(\gamma_{12} - \gamma_{13}) + b_{13}(\gamma_{11} - \gamma_{13}),\\
\mathbf{S}_{21} &= b_{12}(\gamma_{22} - \gamma_{12}) + b_{13}(\gamma_{23} - \gamma_{12}),\\
\mathbf{S}_{22} &= b_{23}(\gamma_{23} - \gamma_{22}) + b_{12}(\gamma_{12} - \gamma_{22}),\\
\mathbf{S}_{23} &= b_{23}(\gamma_{22} - \gamma_{23}) + b_{13}(\gamma_{12} - \gamma_{23}),\\
\mathbf{S}_{31} &= b_{12}(\gamma_{23} - \gamma_{13}) + b_{13}(\gamma_{33} - \gamma_{13}),\\
\mathbf{S}_{32} &= b_{12}(\gamma_{13} - \gamma_{23}) + b_{23}(\gamma_{33} - \gamma_{23}),\\
\mathbf{S}_{33} &= b_{23}(\gamma_{23} - \gamma_{33}) + b_{13}(\gamma_{13} - \gamma_{33}).
\end{aligned} \tag{14}$$

The solution of equation (12) is

$$\mathbf{v}_i(\tau) = \exp(\mathbf{S}\tau)\,\mathbf{v}_i(0), \tag{15}$$

where $\exp(\mathbf{S}\tau)$ can be computed analytically as

$$\exp(\mathbf{S}\,\tau) = \mathbf{I}_3 \; - \; \frac{1 - e^{\lambda_1 \tau}}{\lambda_1}\,\mathbf{S} \; + \; \frac{(1 - e^{\lambda_2 \tau})\lambda_1 - (1 - e^{\lambda_1 \tau})\lambda_2}{\lambda_1 \lambda_2\,(\lambda_1 - \lambda_2)}\,\mathbf{S} \cdot (\mathbf{S} - \lambda_1 \mathbf{I}_3), \tag{16}$$

with $\{0, \lambda_1, \lambda_2\}$ the eigenvalues of matrix $\mathbf{S}$, and $\mathbf{I}_3$ the 3×3 identity matrix. The eigenvalues are

$$\lambda_1 = \frac{1}{2}\left[\mathrm{tr}(\mathbf{S}) - \sqrt{[\mathrm{tr}(\mathbf{S})]^2 - 4E}\right], \qquad \lambda_2 = \mathrm{tr}(\mathbf{S}) - \lambda_1, \tag{17}$$

where

$$E = S_{13}S_{21} - S_{11}S_{23} - S_{13}S_{31} + S_{23}S_{31} + S_{11}S_{33} - S_{21}S_{33}.$$

The regular operator $\exp(\mathbf{M}_r \tau)$ is approximated with a 4th-order Runge Kutta solver. The output vector is

$$\mathbf{w}^{n+1} = \mathbf{w}^* + \frac{\tau}{6}(\Delta_1 + 2\Delta_2 + 2\Delta_3 + \Delta_4), \tag{18}$$

where

$$\begin{aligned}
\Delta_1 &= \mathbf{M}_r\,\mathbf{w}^* + \mathbf{s}^n,\\
\Delta_2 &= \mathbf{M}_r\,(\mathbf{w}^* + \tfrac{\tau}{2}\Delta_1) + \mathbf{s}^{n+1/2},\\
\Delta_3 &= \mathbf{M}_r\,(\mathbf{w}^* + \tfrac{\tau}{2}\Delta_2) + \mathbf{s}^{n+1/2},\\
\Delta_4 &= \mathbf{M}_r\,(\mathbf{w}^* + \tau\Delta_3) + \mathbf{s}^{n+1},
\end{aligned}$$

and $\mathbf{w}^*$ is the intermediate output vector obtained after the operation with the stiff evolution operator. Variables with the superscript n indicate values at time $n\,dt$. The spatial derivatives are calculated with the Fourier method by using the fast Fourier transform [3]. This approximation is infinitely accurate for band limited periodic functions with cutoff spatial wavenumbers which are smaller than the cutoff wavenumbers of the mesh.

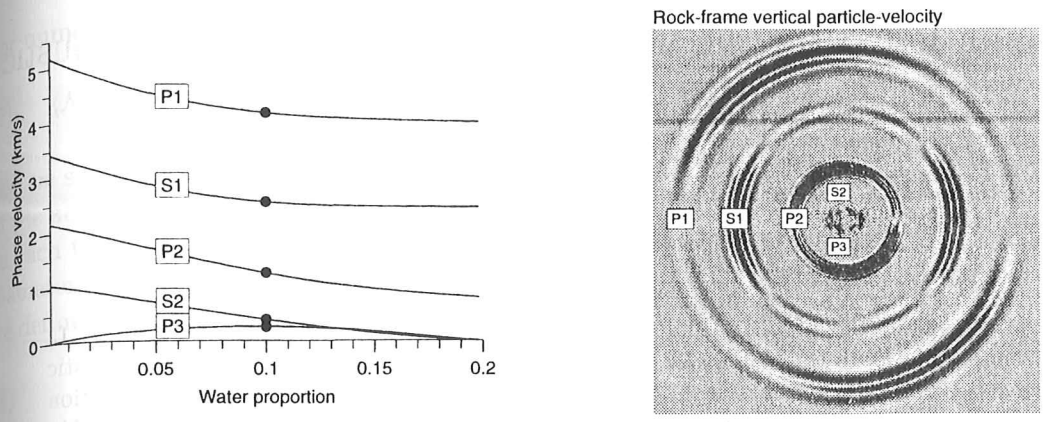

FIG. 1. Left: *Phase velocity versus water proportion of the five waves propagating in a frozen porous medium.* Right: *Snapshot showing the five waves propagating in a frozen porous medium.*

4 Example

Solid grain, ice and water densities and bulk moduli are 2650, 920 and 1000 kg/m^3 and 38.7, 8.6 and 2.25 GPa, respectively; solid grain and ice shear moduli are 39.6 and 33.2 GPa, respectively; rock-frame bulk and shear moduli are 14.4 and 26.1 GPa, respectively. A percolation model is used for the shear modulus of the rock-frame, such that its value at full water saturation is 13.1 GPa. The porosity is 20 %, with 10 % water proportion (50 % water saturation and 50 % ice "saturation"), and we assume no losses due to viscosity effects. We consider a 357 × 357 mesh, with square cells and a grid spacing of 14 m. The perturbation has a dominant frequency of 12.5 Hz and is a combination of bulk source and shear force. Figure 1 (left) shows the phase velocities of the five wave modes versus water proportion, where the compressional waves are labeled P1, P2 and P3, and the shear waves are labeled S1 and S2. The dots indicate the velocities at 50 % water saturation: 4124 m/s for P1, 2511 m/s for S1, 1227 m/s for P2, 386 m/s for S2 and 255 m/s for P3. At full water saturation three wave propagate, and the velocities are those predicted by Biot's theory. A snapshot of the wavefield is shown in Figure 1 (right). Waves S2 and P3 are aliased, since the mesh "supports" a minimum velocity of 700 m/s according to the Nyquist criterion.

These results are preliminary. The research proceeds as follows: i) Wavefield calculation for realistic cases (i.e., including fluid-viscosity effects) and ii) Introduction of viscoelastic effects to model the observed attenuation levels in rocks.

References

[1] J. M. Carcione, and G. Quiroga-Goode, *Some aspects of the physics and numerical modeling of Biot compressional waves*, J. Comput. Acous., 3 (1996), pp. 261-280.

[2] J. M. Carcione, and G. Seriani, *Seismic and ultrasonic velocities in permafrost*, Geophys. Prosp., 46 (1998), pp. 441-454.

[3] B. Fornberg, *A practical guide to pseudospectral methods*, Cambridge University Press (1996).

[4] M. K. Jain., *Numerical solutions of partial differential equations*, Wiley Eastern Ltd. (1984).

[5] P. Lancaster, and M. Tismenetsky, *The theory of matrices*, Academic Press (1985).

[6] P. Leclaire, F. Cohen-Ténoudji, and J. Aguirre-Puente, *Extension of Biot's theory of wave propagation to frozen porous media*, J. Acoust. Soc. Am., 96, (1994), pp. 3753-3768.